Proceedings of the 2014 IEEE
International Conference on Robotics and Biomimetics
December 5-10, 2014, Bali, Indonesia

Robot Control via Output Regulation in Cardiac Surgery

Xiaorui Zhu, Jingdan Min, Wei Lin

***Abstract*—Robot-assisted Cardiac Surgery has remarkably helped surgeons to operate on a beating heart. The robot is preferred to move simultaneously with a point of interest (POI) on the heart surface such that surgeons are enabled to operate as if the heart is stationary. Hence an output regulation technique is proposed in this paper for the surgical robot to track the heart motion without exactly knowing the reference heart motion. Simulations are used to demonstrate its advantage over model predictive control.**

***Index Terms*—Beating heart surgery, surgical robotics, output regulation, tracking.**

I. Introduction

Robot-assisted surgery has readily been the main trend of the surgery. Robot-assisted surgery could benefit both patient and surgeon. It can decrease length of stay, blood loss and analgesic requirements for the patient while allowing the surgeon to operate with less risk of neck and back injury due to ergonomic improvements. Several robotic surgical systems have been authenticated by FDA so far such as the first robotic device to have FDA approval in clinic surgery, AESOP, developed by Computer Motion Company, and da Vinci surgical robot by Intuitive Surgical Company.

Coronary heart disease (CHD) is a common disease of cardiovascular system that could cause serious damage to human body. Coronary artery bypass grafting (CABG) has been one of the effective therapies of CHD for decades. Mostly, cardiopulmonary bypass (heart-lung machine) should to be used in opening heart surgeries to temporarily take over the function of the heart, which is so called "on-pump surgery". However, it is believed by the medical community that cardiopulmonary bypass could cause a post-operative cognitive decline. Therefore off-pump surgery is chosen by some well-trained surgeons where the heart is still beating during surgery. But off-pump surgery can be more technically challenging and require more training and experience in order to achieve similar results as on-pump surgery.

In the robot assisted cardiac surgery, the robotic arm equipped with cameras can be used to operate on the beating heart while the surgeon operates remotely. The surgeon observing the surgical site through the camera can see a relatively motionless image of the heart [1]. At the same time, a surgical robot can be used to track the motion of the heart such that the surgeon could operate as if the heart was stationary. Unlike conventional off-pump CABG surgery, the robot in such robot-assisted surgery system can be used to automatically eliminate the relative motion between the heart and robot by motion compensation algorithms.

A few research groups have made great efforts in estimating and tracking relative motion of the heart. Thakral et al. [2] proposed non-stationary Fourier series for modeling heart motion and then used the least square method to identify each parameter of heart motion model. Ortmaier et al. [3] developed a new prediction scheme using the fusion of biological signals Electrocardiography (ECG) and Respiration (RSP) in the estimation algorithms and applying model predictive control (MPC) approach for tracking to improve the robustness in case of disturbance or occlusion. Ginhouxet al. [4] presented a new MPC-based approach for tracking of a beating heart where the heart motion was separated from respiratory motion and then predicted by estimating the frequencies, amplitude and phase of the harmonics. Rotella [5] proposed a new strategy to use the previous cycle of heart motion data as heart motion estimation of the current cycle. Bebek et al [6] improved Rotella's prediction algorithm using ECG data to correct the period of heart motion, and then proposed a receding horizon model predictive control (RHMPC) approach to improve tracking performance of surgical robot. Cagneau et al [7] developed a force feedback control scheme with iterative learning controller for compensating physiological heart motions assuming the periodic disturbance. However the assumption of periodicity was an oversimplification of the actual heart motion. Duindam et al [8] proposed a full 3-D heart motion model and an adaptive model predictive controller for motion compensation to adapt to the entire heart surface. Yuen et al. [9] presented a 3D ultrasound-guided motion compensation for beating heart mitral repair to reduce the impact of tracking delay and noise. Florez et al [10] incorporated a locally weighted projection regression (LWPR) based identification into a model-based predictive force control law in order to heighten the level of controller robustness in beating heart surgery. However, their assumption of the periodic ECG signal was an oversimplication. Although the above predictive controllers are promising, the performances remained limited by the need for correct perturbation estimation [11].

It was found that fundamental frequencies of heart motion are stable in a short period for an individual. Therefore an output regulation approach is proposed in this paper to achieve motion compensation without fully estimating the heart motion because output regulation can deal with tracking problems without knowing exact estimation of the references. Only fundamental frequencies need to be estimated from the previous cycle of ECG in the proposed technique. Then the heart motion can be treated as a family of trajectories

This research is currently supported by the National Science and Technology Ministry of China under Grant No. 2013BAK01B02, and by Shenzhen Key Lab on Wind Energy and Smart Grids (CXB201005250025A), and Research Projects JC201104210048A, JC201105160551A, KQC201105300002A and JCY201303291521257.

Xiaorui Zhu is the corresponding author with Harbin Institute of Technology Shenzhen Graduate School, Shenzhen, Guangdong 518055, China (e-mail: xiaoruizhu@hitsz.edu.cn).

Wei Lin is with Case Western Reserve University, Cleveland, OH, USA (e-mail: linwei@case.edu).

978-1-4799-7397-2/14/$31.00 © 2014 IEEE

generated by a differential equation. Hence an output regulator can be designed based on the estimated frequencies of the precious cycle to track heart motion at the current cycle.

The rest of this paper is arranged as follows. Heart motion is modelled in Section II. In section III, an output regulator is designed for tracking heart motion. Simulation results are presented in Section IV. Conclusions are made in Section V.

II. Modelling of Heart Motion

In general, heart motion can be modelled as the sum of the respiratory and cardiac motions using a dual Fourier series as [12],

$$f(k;\boldsymbol{x}) = c + \sum_{i=1}^{N_r}\left[a_{r,i}\sin(i\omega_r k\Delta T) + b_{r,i}\cos(i\omega_r k\Delta T)\right] + \sum_{j=1}^{N_c}\left[a_{c,j}\sin(j\omega_r k\Delta T) + b_{c,j}\cos(j\omega_r k\Delta T)\right] \quad (1)$$

where ΔT is the sampling period, N_r and N_c are the numbers of harmonics for the respiratory and cardiac components respectively. ω_r and ω_c are the respiratory and cardiac frequencies. $\boldsymbol{x} = [\omega_r\Delta T, \omega_c\Delta T, c,\ a_{r,1},\cdots,a_{r,N_r}, a_{c,1},\cdots, a_{c,N_c}, b_{r,1},\cdots,b_{r,N_r}, b_{c,1},\cdots,b_{c,N_c}]$ is defined as the coefficient vector. However, according to the literature [13], there is also a coupling between cardiac and respiratory activities such as peak amplitudes at frequencies of $\omega_c \pm \omega_r$, $2\omega_c \pm \omega_r$, etc.. In order to represent heart motion more precisely, a coupled dual Fourier series model will be applied in this paper as,

$$f(k;\boldsymbol{x}) = c + \sum_{i=1}^{N_r}\left[a_{r,i}\sin(i\omega_r k\Delta T) + b_{r,i}\cos(i\omega_r k\Delta T)\right] + \sum_{j=1}^{N_c}\left[a_{c,j}\sin(j\omega_c k\Delta T) + b_{c,j}\cos(j\omega_c k\Delta T)\right] + \sum_{m=1}^{N_h}\left[a_{h1,m}\sin\big((m\omega_c-\omega_r)k\Delta T\big) + b_{h1,m}\cos\big((m\omega_c-\omega_r)k\Delta T\big)\right] + \sum_{n=1}^{N_h}\left[a_{h2,n}\sin\big((n\omega_c+\omega_r)k\Delta T\big) + b_{h2,n}\cos\big((n\omega_c+\omega_r)k\Delta T\big)\right] \quad (2)$$

where N_h is the half of the number of coupled harmonics for modeling heart motion, $a_{h1,m}$, $a_{h2,n}$, $b_{h1,m}$, and $b_{h2,n}$ $(m,n = 1,\cdots,N_h)$ are corresponding coefficients. In Eq. (2), the coefficient vector, $\boldsymbol{x}$, is defined as $[\omega_r\Delta T, \omega_c\Delta T, c, a_{r,1},\cdots,a_{r,N_r}, a_{c,1},\cdots,a_{c,N_c}, a_{h1,1},\cdots,a_{h1,N_h}, a_{h2,1},\cdots,a_{h2,N_h}, b_{r,1},\cdots,b_{r,N_r}, b_{c,1},\cdots,b_{c,N_c}, b_{h2,1},\cdots,b_{h2,N_h}, b_{h2,1},\cdots,b_{h2,N_h}]$. Note that N_h is not greater than N_c.

In this paper, the Levenberg-Marquardt algorithm (LMA) is used to identify the fundamental frequencies of the Fourier series because LMA can make the estimation error decay to a small value even with large initial estimation errors. Assume that the measurement is the sum of Fourier series and a white noise. Define $\boldsymbol{Y}$ as the vector of measured heart positions, and $\boldsymbol{F}(\boldsymbol{x})$ as the vector of the estimated positions.

$$\boldsymbol{Y} = [y_{\text{mea}}(1) \quad y_{\text{mea}}(2) \quad \cdots \quad y_{\text{mea}}(L)]^T \quad (3)$$

$$\boldsymbol{F}(\boldsymbol{x}) = [f(1;\boldsymbol{x}) \quad f(2;\boldsymbol{x}) \quad \cdots \quad f(L;\boldsymbol{x})]^T \quad (4)$$

where L is length of the heart data in a given short time period, and $y_{\text{mea}}(i)$ and $f(i;\boldsymbol{x})$ are respectively measurement and estimation of heart motion at the i-th sampling period for $i = 1,\cdots,L$. LMA can be computed using the following iteration:

$$\hat{\boldsymbol{x}}(n+1) = \hat{\boldsymbol{x}}(n) + (\boldsymbol{D}^T\boldsymbol{D} + \lambda\boldsymbol{I})^{-1}\boldsymbol{D}^T\left(\boldsymbol{Y} - \boldsymbol{F}(\hat{\boldsymbol{x}}(n))\right) \quad (5)$$

where $\hat{\boldsymbol{x}}(n)$ is estimation of the parameter vector at the n-th iteration, $\boldsymbol{D}$ is the Jacobian matrix of $\boldsymbol{F}(x)$, and λ is the damping parameter that can be adjusted for a better iteration.

III. Design of Output Regulator

A. Problem formulation

The objective of this paper is to design an output feedback control law for a robot assisted surgery to track heart motion. Let $\boldsymbol{\theta}$ and $\dot{\boldsymbol{\theta}}$ denote angular position vector and angular velocity vector of robot joints respectively. Then the robotic manipulator can be modeled by the equation [14],

$$\boldsymbol{M}(\boldsymbol{\theta})\ddot{\boldsymbol{\theta}} + \boldsymbol{C}(\boldsymbol{\theta},\dot{\boldsymbol{\theta}})\dot{\boldsymbol{\theta}} + \boldsymbol{N}(\boldsymbol{\theta}) = \boldsymbol{\tau} \quad (6)$$

where $\boldsymbol{M}(\boldsymbol{\theta})$ denotes the inertia matrix of the surgical robot, $\boldsymbol{C}(\boldsymbol{\theta},\dot{\boldsymbol{\theta}})$ denotes the Coriolis matrix, and $\boldsymbol{N}(\boldsymbol{\theta})$ is the gravity vector. Choose $\boldsymbol{\theta}_1 = \boldsymbol{\theta}$ and $\boldsymbol{\theta}_2 = \dot{\boldsymbol{\theta}}$, and then the following state equations can be obtained as,

$$\dot{\boldsymbol{\theta}}_1 = \boldsymbol{\theta}_2 \quad (7)$$

$$\dot{\boldsymbol{\theta}}_2 = \big(\boldsymbol{M}(\boldsymbol{\theta}_1)\big)^{-1}\big(\boldsymbol{\tau} - \boldsymbol{C}(\boldsymbol{\theta}_1,\boldsymbol{\theta}_2)\boldsymbol{\theta}_2 - \boldsymbol{N}(\boldsymbol{\theta}_1)\big) \quad (8)$$

$$\boldsymbol{y} = \boldsymbol{p}(\boldsymbol{\theta}_1) \quad (9)$$

where $\boldsymbol{p}(\boldsymbol{\theta}_1)$ is the end effector position of the surgical robot. Note that the equilibrium point of the system is not the origin when the torque input $\boldsymbol{\tau} = \boldsymbol{0}$. Hence a new input $\boldsymbol{u} = \boldsymbol{\tau} - \boldsymbol{N}(\boldsymbol{0})$ is introduced to transform the state equations of the system as,

$$\dot{\boldsymbol{\theta}}_1 = \boldsymbol{\theta}_2 \quad (10)$$

$$\dot{\boldsymbol{\theta}}_2 = \boldsymbol{f}_1(\boldsymbol{\theta}_1,\boldsymbol{\theta}_2) + \boldsymbol{g}_1(\boldsymbol{\theta}_1)\boldsymbol{u} \quad (11)$$

$$\boldsymbol{y} = \boldsymbol{p}(\boldsymbol{\theta}_1) \quad (12)$$

where

$$\boldsymbol{f}_1(\boldsymbol{\theta}_1,\boldsymbol{\theta}_2) = \big(\boldsymbol{M}(\boldsymbol{\theta}_1)\big)^{-1}\boldsymbol{C}(\boldsymbol{\theta}_1,\boldsymbol{\theta}_2)\boldsymbol{\theta}_2 \quad (13)$$

$$\boldsymbol{g}_1(\boldsymbol{\theta}_1) = \big(\boldsymbol{M}(\boldsymbol{\theta}_1)\big)^{-1}. \quad (14)$$

Define the trajectory of the real heart motion as the reference output of the proposed motion compensation system denoted by $\boldsymbol{y}_{\text{ref}}$. Assume this reference output can be represented as,

$$\boldsymbol{y}_{\text{ref}} = \boldsymbol{q}(\boldsymbol{w}) \quad (15)$$

where $\boldsymbol{w}$ is a set of exogenous inputs generated by a linear time-invariant exosystem. This exosystem can be written as,

$$\dot{\boldsymbol{w}} = \boldsymbol{s}(\boldsymbol{w}) \quad (16)$$

with the initial condition $\boldsymbol{w}(0)$ ranging on some neighborhood of the origin. As mentioned in Section II, the real heart motion can be modeled as summation of a number of harmonics. Hence the frequencies and phases of each harmonic in the reference output will be determined by an exosystem such as Eq. (16). By property of sinuous signal, the reference output can be generated by the following exosystem:

$$\begin{aligned} \dot{\boldsymbol{w}}_0 &= \boldsymbol{0} \\ \dot{\boldsymbol{w}}_i &= \boldsymbol{w}_{i+N} \\ \dot{\boldsymbol{w}}_{i+N} &= -\Omega_i^2 \boldsymbol{w}_i \\ (i &= 1, \cdots, N) \end{aligned} \tag{17}$$

$$\boldsymbol{y}_{\text{ref}} = \boldsymbol{w}_0 + \boldsymbol{w}_1 + \cdots + \boldsymbol{w}_N \tag{18}$$

where $\boldsymbol{w}_i \in \mathbb{R}^3$ $(i = 0, \cdots, 2N)$. Define $\boldsymbol{\Omega}$ as

$$\boldsymbol{\Omega} = \begin{bmatrix} -\Omega_1^2 \boldsymbol{I}_{3\times3} & \cdots & \boldsymbol{0} \\ \vdots & \ddots & \vdots \\ \boldsymbol{0} & \cdots & -\Omega_N^2 \boldsymbol{I}_{3\times3} \end{bmatrix}.$$

Then $\boldsymbol{s}(\boldsymbol{w})$ can be rewritten as,

$$\boldsymbol{s}(\boldsymbol{w}) = \boldsymbol{S}\boldsymbol{w}$$

where

$$\boldsymbol{S} = \begin{bmatrix} \boldsymbol{0}_{3\times3} & \boldsymbol{0}_{3\times3N} & \boldsymbol{0}_{3\times3N} \\ \boldsymbol{0}_{3N\times3} & \boldsymbol{0}_{3N\times3N} & \boldsymbol{I}_{3N\times3N} \\ \boldsymbol{0}_{3N\times3} & \boldsymbol{\Omega}_{3N\times3N} & \boldsymbol{0}_{3N\times3N} \end{bmatrix}.$$

Likewise, $\boldsymbol{q}(\boldsymbol{w})$ can be rewritten as,

$$\boldsymbol{q}(\boldsymbol{w}) = \boldsymbol{Q}\boldsymbol{w}$$

where

$$\boldsymbol{Q} = \left[\underbrace{\boldsymbol{I}_{3\times3} \quad \cdots \quad \boldsymbol{I}_{3\times3}}_{N+1} \quad \boldsymbol{0}_{3\times N}\right].$$

Hence it is easy to prove that $\boldsymbol{w} = \boldsymbol{0}$ is a neutrally stable equilibrium of the above exosystem.

Define the error $\boldsymbol{e}$ as,

$$\boldsymbol{e} = \boldsymbol{y} - \boldsymbol{y}_{\text{ref}} = \boldsymbol{p}(\boldsymbol{\theta}_1) - \boldsymbol{q}(\boldsymbol{w}) \tag{19}$$

Then the new state equations of the system become

$$\dot{\boldsymbol{\theta}}_1 = \boldsymbol{\theta}_2 \tag{20}$$

$$\dot{\boldsymbol{\theta}}_2 = \boldsymbol{f}_1(\boldsymbol{\theta}_1, \boldsymbol{\theta}_2) + \boldsymbol{g}_1(\boldsymbol{\theta}_1)\boldsymbol{u} \tag{21}$$

$$\dot{\boldsymbol{w}} = \boldsymbol{s}(\boldsymbol{w}) \tag{22}$$

$$\boldsymbol{e} = \boldsymbol{p}(\boldsymbol{\theta}_1) - \boldsymbol{q}(\boldsymbol{w}). \tag{23}$$

Therefore such error feedback output regulation problem is to find mappings $\boldsymbol{\theta}_1 = \boldsymbol{\pi}_1(\boldsymbol{w})$, $\boldsymbol{\theta}_2 = \boldsymbol{\pi}_2(\boldsymbol{w})$ and $\boldsymbol{u} = \boldsymbol{c}(\boldsymbol{w})$ with $\boldsymbol{\pi}_1(\boldsymbol{0}) = \boldsymbol{0}$, $\boldsymbol{\pi}_2(\boldsymbol{0}) = \boldsymbol{0}$, and $\boldsymbol{c}(\boldsymbol{0}) = \boldsymbol{0}$ defined in a neighborhood of the origin, satisfying the following equations,

$$\frac{\partial \boldsymbol{\pi}_1}{\partial \boldsymbol{w}} \boldsymbol{s}(\boldsymbol{w}) = \boldsymbol{\pi}_2(\boldsymbol{w}) \tag{24}$$

$$\frac{\partial \boldsymbol{\pi}_2}{\partial \boldsymbol{w}} \boldsymbol{s}(\boldsymbol{w}) = \boldsymbol{f}_1\big(\boldsymbol{\pi}_1(\boldsymbol{w}), \boldsymbol{\pi}_2(\boldsymbol{w})\big) + \boldsymbol{g}_1\big(\boldsymbol{\pi}_1(\boldsymbol{w})\big)\boldsymbol{c}(\boldsymbol{w}) \tag{25}$$

$$\boldsymbol{p}\big(\boldsymbol{\pi}_1(\boldsymbol{w})\big) - \boldsymbol{q}(\boldsymbol{w}) = \boldsymbol{0} \tag{26}$$

Because the relative motion between the heart and end-effector of the surgical robot, $\boldsymbol{e}$, can be measured only, internal state $\boldsymbol{z} = \boldsymbol{\rho}(\boldsymbol{w})$ with $\boldsymbol{\rho}(\boldsymbol{0}) = \boldsymbol{0}$ also need to be found such that $\boldsymbol{z}$ can be modeled by an auxiliary autonomous system [15] as,

$$\dot{\boldsymbol{z}} = \boldsymbol{\phi}(\boldsymbol{z}) \tag{27}$$

$$\boldsymbol{u} = \boldsymbol{\gamma}(\boldsymbol{z}) \tag{28}$$

satisfying the immersion conditions

$$\frac{\partial \boldsymbol{\rho}}{\partial \boldsymbol{w}} \boldsymbol{S}\boldsymbol{w} = \boldsymbol{\phi}\big(\boldsymbol{\rho}(\boldsymbol{w})\big) \tag{29}$$

$$\boldsymbol{c}(\boldsymbol{w}) = \boldsymbol{\gamma}\big(\boldsymbol{\rho}(\boldsymbol{w})\big) \tag{30}$$

where Eq. (27) can be treated as an observer of the state $\boldsymbol{w}$, also known as the internal model.

B. Design of the internal model

It is easy to prove that the following propositions hold.

P1: The pair $\left[\begin{matrix} \boldsymbol{\theta}_2 \\ \boldsymbol{f}_1(\boldsymbol{\theta}_1, \boldsymbol{\theta}_2) \end{matrix}\right]$, $\left[\begin{matrix} \boldsymbol{0} \\ \boldsymbol{g}_1(\boldsymbol{\theta}_1) \end{matrix}\right]$ has a stabilizable linear approximation at $\left[\begin{matrix} \boldsymbol{\theta}_1 \\ \boldsymbol{\theta}_2 \end{matrix}\right] = \left[\begin{matrix} \boldsymbol{0} \\ \boldsymbol{0} \end{matrix}\right]$;

P2: The pair $\boldsymbol{s}(\boldsymbol{w})$, $\boldsymbol{q}(\boldsymbol{w})$ has a detectable linear approximation at $\boldsymbol{w} = \boldsymbol{0}$.

Because of the triangular structure of the system, the solution of the regulation equations can be set as,

$$\boldsymbol{\pi}_1(\boldsymbol{w}) = \boldsymbol{\theta}_{\text{ref}} \tag{31}$$

$$\boldsymbol{\pi}_2(\boldsymbol{w}) = \dot{\boldsymbol{\theta}}_{\text{ref}} \tag{32}$$

$$\boldsymbol{c}(\boldsymbol{w}) = \boldsymbol{M}(\boldsymbol{\theta}_{\text{ref}})\ddot{\boldsymbol{\theta}}_{\text{ref}} + \boldsymbol{C}\big(\boldsymbol{\theta}_{\text{ref}}, \dot{\boldsymbol{\theta}}_{\text{ref}}\big)\dot{\boldsymbol{\theta}}_{\text{ref}} + \boldsymbol{N}(\boldsymbol{\theta}_{\text{ref}}) \tag{33}$$

where $\boldsymbol{\theta}_{\text{ref}} = \boldsymbol{p}^{-1}(\boldsymbol{Q}\boldsymbol{w})$, $\dot{\boldsymbol{\theta}}_{\text{ref}} = \frac{\mathrm{d}}{\mathrm{dt}}\boldsymbol{\theta}_{\text{ref}}$ and $\ddot{\boldsymbol{\theta}}_{\text{ref}} = \frac{\mathrm{d}}{\mathrm{dt}}\dot{\boldsymbol{\theta}}_{\text{ref}}$ represent angular positions, velocities and accelerations of the robot joints respectively. However, the exosystem $\dot{\boldsymbol{w}} = \boldsymbol{s}(\boldsymbol{w})$ cannot be directly used for controller design because $\boldsymbol{w}$ is not observable. So an internal model $\dot{\boldsymbol{z}} = \boldsymbol{\phi}(\boldsymbol{z})$ will be constructed by introducing a transformation $\boldsymbol{z} = \boldsymbol{\rho}(\boldsymbol{w})$. It is noticed that the forward kinematics of robot describes the relationship between the Cartesian coordinates and joint angles. Hence the forward kinematics can be used as the transformation $\boldsymbol{z} = \boldsymbol{\rho}(\boldsymbol{w})$ to transform $\boldsymbol{w}$ in the Cartesian space to $\boldsymbol{z}$ in the joint space. Then the reference output becomes a function of $\boldsymbol{z}$ as,

$$\boldsymbol{y}_{\text{ref}} = \boldsymbol{w}_0 + \cdots + \boldsymbol{w}_N = \boldsymbol{p}(\boldsymbol{z}_0 + \cdots + \boldsymbol{z}_N) = \boldsymbol{p}(\boldsymbol{\theta}_{\text{ref}}) \tag{34}$$

For convenience, each element of the vector $\boldsymbol{z}$ is designed to correspond respectively to harmonics represented by each element in $\boldsymbol{w}$.

$$\begin{aligned} \boldsymbol{w}_0 &= \boldsymbol{p}(\boldsymbol{z}_0) \\ \boldsymbol{w}_i &= \boldsymbol{p}(\boldsymbol{z}_0 + \cdots + \boldsymbol{z}_i) - \boldsymbol{p}(\boldsymbol{z}_0 + \cdots + \boldsymbol{z}_{i-1}) \\ \boldsymbol{w}_{i+N} &= \boldsymbol{J}(\boldsymbol{z}_0 + \cdots + \boldsymbol{z}_i)(\boldsymbol{z}_{N+1} + \cdots + \boldsymbol{z}_{N+i}) \\ &\quad - \boldsymbol{J}(\boldsymbol{z}_0 + \cdots + \boldsymbol{z}_{i-1})(\boldsymbol{z}_{N+1} + \cdots \\ &\quad + \boldsymbol{z}_{N+i-1}) \\ (\boldsymbol{i} &= 1, \cdots, N) \end{aligned} \tag{35}$$

Clearly, the transformation $\boldsymbol{z} = \boldsymbol{\rho}(\boldsymbol{w})$ is a diffeomorphism in a neighborhood of the origin whose inverse $\boldsymbol{w} = \boldsymbol{\rho}^{-1}(\boldsymbol{z})$ is depicted by Eq. (35). Then substituting $\boldsymbol{z} = \boldsymbol{\rho}(\boldsymbol{w})$ into Eqs. (29) and (30) yields

$$\boldsymbol{\phi}(\boldsymbol{z}) = \left(\frac{\partial \boldsymbol{\rho}}{\partial \boldsymbol{z}}\right)^{-1} \boldsymbol{S}\boldsymbol{\rho}(\boldsymbol{z}) \tag{36}$$

$$\boldsymbol{\gamma}(\boldsymbol{z}) = \boldsymbol{c}\big(\boldsymbol{\rho}(\boldsymbol{z})\big) \tag{37}$$

According to Eqs. (34) and (35),

$$\boldsymbol{\theta}_{\text{ref}} = \boldsymbol{z_0} + \cdots + \boldsymbol{z_N} = \boldsymbol{R_1 z} \tag{38}$$

$$\dot{\boldsymbol{\theta}}_{\text{ref}} = \boldsymbol{z_{N+1}} + \cdots + \boldsymbol{z_{2N}} = \boldsymbol{R_2 z} \tag{39}$$

$$\ddot{\boldsymbol{\theta}}_{\text{ref}} = \boldsymbol{\Phi}(\boldsymbol{z}) \triangleq \boldsymbol{\phi_1}(\boldsymbol{z}) + \cdots + \boldsymbol{\phi_{N+1}}(\boldsymbol{z}) \tag{40}$$

where

$$\boldsymbol{R}_1 = \Big[\underbrace{\boldsymbol{I}_{3\times3} \quad \cdots \quad \boldsymbol{I}_{3\times3}}_{N+1} \quad \boldsymbol{0}_{3\times N}\Big]$$

$$\boldsymbol{R}_2 = \Big[\boldsymbol{0}_{3\times(N+1)} \quad \underbrace{\boldsymbol{I}_{3\times3} \quad \cdots \quad \boldsymbol{I}_{3\times3}}_{N}\Big]$$

Since $\boldsymbol{\gamma}(\boldsymbol{z}) = \boldsymbol{c}(\boldsymbol{w})$, substituting Eqs. (38)–(40) into Eq. (33) yields

$$\boldsymbol{\gamma}(\boldsymbol{z}) = \boldsymbol{M}(\boldsymbol{R_1 z})\boldsymbol{\Phi}(\boldsymbol{z}) + \boldsymbol{C}(\boldsymbol{R_1 z}, \boldsymbol{R_2 z})\boldsymbol{R_2 z} + \boldsymbol{N}(\boldsymbol{R_1 z}) \tag{41}$$

Thus, we have obtained the autonomous system satisfying immerse condition in the regulation problem.

$$\boldsymbol{\tau} = \boldsymbol{\gamma}(\boldsymbol{z}) + \boldsymbol{K}_1(\boldsymbol{\theta}_1 - \boldsymbol{R}_1\boldsymbol{z}) + \boldsymbol{K}_2(\boldsymbol{\theta}_2 - \boldsymbol{R}_2\boldsymbol{z}) \tag{42}$$

$$\dot{\boldsymbol{z}} = \boldsymbol{\phi}(\boldsymbol{z}) + \boldsymbol{G}\big(\boldsymbol{p^{-1}}\big(\boldsymbol{y_{ref}}\big) - \boldsymbol{R_1 z}\big) \tag{43}$$

where $\boldsymbol{K}_1$, $\boldsymbol{K}_2$, and $\boldsymbol{G}$ are proper matrices to make the controlled system converge. Contrasting Eqs. (38) and (39) with Eqs. (31) and (32) gives

$$\boldsymbol{R}_1\boldsymbol{z} = \boldsymbol{\pi}_1\big(\boldsymbol{\rho}^{-1}(\boldsymbol{z})\big) \tag{44}$$

$$\boldsymbol{R}_2\boldsymbol{z} = \boldsymbol{\pi}_2\big(\boldsymbol{\rho}^{-1}(\boldsymbol{z})\big) \tag{45}$$

Hence, control law of the output regulator has the following form

$$\begin{aligned}\boldsymbol{\tau} = \boldsymbol{c}\big(\boldsymbol{\rho}^{-1}(\boldsymbol{z})\big) &+ \boldsymbol{K}_1\Big(\boldsymbol{\theta}_1 - \boldsymbol{\pi}_1\big(\boldsymbol{\rho}^{-1}(\boldsymbol{z})\big)\Big) \\ &+ \boldsymbol{K}_2\Big(\boldsymbol{\theta}_2 - \boldsymbol{\pi}_2\big(\boldsymbol{\rho}^{-1}(\boldsymbol{z})\big)\Big)\end{aligned} \tag{46}$$

$$\begin{aligned}\dot{\boldsymbol{z}} = \left(\frac{\partial\boldsymbol{\rho}^{-1}}{\partial\boldsymbol{z}}\right)^{-1} &\boldsymbol{s}\big(\boldsymbol{\rho}^{-1}(\boldsymbol{z})\big) \\ &+ \boldsymbol{G}\Big(\boldsymbol{p}^{-1}\big(\boldsymbol{q}(\boldsymbol{w})\big) - \boldsymbol{\pi}_1\big(\boldsymbol{\rho}^{-1}(\boldsymbol{z})\big)\Big)\end{aligned} \tag{47}$$

Claim: The feedback controller of Eqs. (46) and (47) can solve the regulation problem with the system of Eqs. (20) to (23).

Proof: Combining Eqs. (20), (21), (22), (46) and (47) yields a closed-loop system as,

$$\dot{\boldsymbol{\theta}}_1 = \boldsymbol{\theta}_2 \tag{48}$$

$$\begin{aligned}\dot{\boldsymbol{\theta}}_2 = \boldsymbol{f}(\boldsymbol{\theta}_1, \boldsymbol{\theta}_2) + \boldsymbol{g}(\boldsymbol{\theta}_1)\Bigg(&\boldsymbol{c}\big(\boldsymbol{\rho}^{-1}(\boldsymbol{z})\big) \\ &+ [\boldsymbol{K}_1 \quad \boldsymbol{K}_2]\begin{bmatrix}\boldsymbol{\theta}_1 - \boldsymbol{\pi}_1\big(\boldsymbol{\rho}^{-1}(\boldsymbol{z})\big) \\ \boldsymbol{\theta}_2 - \boldsymbol{\pi}_2\big(\boldsymbol{\rho}^{-1}(\boldsymbol{z})\big)\end{bmatrix}\Bigg)\end{aligned} \tag{49}$$

$$\begin{aligned}\dot{\boldsymbol{z}} = \left(\frac{\partial\boldsymbol{\rho}^{-1}}{\partial\boldsymbol{z}}\right)^{-1} &\boldsymbol{s}\big(\boldsymbol{\rho}^{-1}(\boldsymbol{z})\big) \\ &+ \boldsymbol{G}\Big(\boldsymbol{p}^{-1}\big(\boldsymbol{q}(\boldsymbol{w})\big) - \boldsymbol{\pi}_1\big(\boldsymbol{\rho}^{-1}(\boldsymbol{z})\big)\Big)\end{aligned} \tag{50}$$

$$\dot{\boldsymbol{w}} = \boldsymbol{s}(\boldsymbol{w}) \tag{51}$$

Then the linear approximation of the closed-loop system can be obtained as,

$$\begin{bmatrix}\dot{\boldsymbol{\theta}}_1 \\ \dot{\boldsymbol{\theta}}_2 \\ \dot{\boldsymbol{z}} \\ \dot{\boldsymbol{w}}\end{bmatrix} = \begin{bmatrix}\boldsymbol{0} & \boldsymbol{I} & \boldsymbol{0} & \boldsymbol{0} \\ \boldsymbol{A}_1 + \boldsymbol{B}_1\boldsymbol{K}_1 & \boldsymbol{A}_2 + \boldsymbol{B}_1\boldsymbol{K}_2 & \boldsymbol{B}_1(\boldsymbol{\Gamma} - \boldsymbol{K}_1\boldsymbol{\Pi}_1 - \boldsymbol{K}_2\boldsymbol{\Pi}_2)\boldsymbol{\Sigma}^{-1} & \boldsymbol{0} \\ \boldsymbol{0} & \boldsymbol{0} & (\boldsymbol{\Sigma S} - \boldsymbol{G\Pi}_1)\boldsymbol{\Sigma}^{-1} & \boldsymbol{G}\boldsymbol{C}_1^{-1}\boldsymbol{Q} \\ \boldsymbol{0} & \boldsymbol{0} & \boldsymbol{0} & \boldsymbol{S}\end{bmatrix}\begin{bmatrix}\boldsymbol{\theta}_1 \\ \boldsymbol{\theta}_2 \\ \boldsymbol{z} \\ \boldsymbol{w}\end{bmatrix} \tag{52}$$

where $\boldsymbol{A}_1$, $\boldsymbol{A}_2$, $\boldsymbol{B}_1$, $\boldsymbol{C}_1$, $\boldsymbol{S}$, $\boldsymbol{Q}$, $\boldsymbol{\Pi}_1$, $\boldsymbol{\Pi}_2$, $\boldsymbol{\Gamma}$, and $\boldsymbol{\Sigma}$ are defined by the following equations:

$$\boldsymbol{A}_1 = \left[\frac{\partial\boldsymbol{f}_1}{\partial\boldsymbol{\theta}_1}\right]_{\boldsymbol{\theta}_1=0,\ \boldsymbol{\theta}_2=0} \quad \boldsymbol{A}_2 = \left[\frac{\partial\boldsymbol{f}_1}{\partial\boldsymbol{\theta}_2}\right]_{\boldsymbol{\theta}_1=0,\ \boldsymbol{\theta}_2=0} \quad \boldsymbol{B}_1 = \boldsymbol{g}_1(\boldsymbol{0})$$

$$\boldsymbol{C}_1 = \left[\frac{\partial\boldsymbol{p}}{\partial\boldsymbol{\theta}_1}\right]_{\boldsymbol{\theta}_1=0} \quad \boldsymbol{S} = \left[\frac{\partial\boldsymbol{s}}{\partial\boldsymbol{w}}\right]_{\boldsymbol{w}=0} \quad \boldsymbol{Q} = \left[\frac{\partial\boldsymbol{q}}{\partial\boldsymbol{w}}\right]_{\boldsymbol{w}=0}$$

$$\boldsymbol{\Pi}_1 = \left[\frac{\partial\boldsymbol{\pi}_1}{\partial\boldsymbol{w}}\right]_{\boldsymbol{w}=0} \quad \boldsymbol{\Pi}_2 = \left[\frac{\partial\boldsymbol{\pi}_2}{\partial\boldsymbol{w}}\right]_{\boldsymbol{w}=0} \quad \boldsymbol{\Gamma} = \left[\frac{\partial\boldsymbol{c}}{\partial\boldsymbol{w}}\right]_{\boldsymbol{w}=0}$$

$$\boldsymbol{\Sigma} = \left[\frac{\partial\boldsymbol{\rho}}{\partial\boldsymbol{w}}\right]_{\boldsymbol{w}=0}\left(\Rightarrow \boldsymbol{\Sigma^{-1}} = \left[\frac{\partial\boldsymbol{\rho}^{-1}}{\partial\boldsymbol{z}}\right]_{\boldsymbol{w}=0}\right)$$

According to *P1*, there exists $\boldsymbol{K}_1$ and $\boldsymbol{K}_2$ such that

$$\boldsymbol{\sigma}\left(\begin{bmatrix}\boldsymbol{0} & \boldsymbol{I} \\ \boldsymbol{A}_1 + \boldsymbol{B}_1\boldsymbol{K}_1 & \boldsymbol{A}_2 + \boldsymbol{B}_1\boldsymbol{K}_2\end{bmatrix}\right) \subset \mathbb{C}^-$$

According to *P2*, there exists $\boldsymbol{G}_0$ such that $\boldsymbol{\sigma}(\boldsymbol{S} - \boldsymbol{G}_0\boldsymbol{Q}) \subset \mathbb{C}^-$. Likewise there exists $\boldsymbol{G}_0$ satisfying

$$\boldsymbol{\sigma}(\boldsymbol{\Sigma}(\boldsymbol{S} - \boldsymbol{G}_0\boldsymbol{Q})\boldsymbol{\Sigma}^{-1}) \subset \mathbb{C}^-$$

Notice that $\boldsymbol{p}\big(\boldsymbol{\pi}_1(\boldsymbol{w})\big) - \boldsymbol{q}(\boldsymbol{w}) = \boldsymbol{0}$ implies $\boldsymbol{Q} = \boldsymbol{C}_1\boldsymbol{\Pi}_1$. Then the following term can be rewritten as,

$$\boldsymbol{\Sigma}(\boldsymbol{S} - \boldsymbol{G}_0\boldsymbol{Q})\boldsymbol{\Sigma}^{-1} = (\boldsymbol{\Sigma S} - \boldsymbol{\Sigma G}_0\boldsymbol{C}_1\boldsymbol{\Pi}_1)\boldsymbol{\Sigma}^{-1}$$

Choose $\boldsymbol{G} = \boldsymbol{\Sigma G}_0\boldsymbol{C}_1$ and then $\boldsymbol{\sigma}\big((\boldsymbol{\Sigma S} - \boldsymbol{G\Pi}_1)\boldsymbol{\Sigma}^{-1}\big) \subset \mathbb{C}^-$.

Hence,

$$\boldsymbol{\sigma}\left(\begin{bmatrix}\boldsymbol{0} & \boldsymbol{I} & \boldsymbol{0} \\ \boldsymbol{A}_1 + \boldsymbol{B}_1\boldsymbol{K}_1 & \boldsymbol{A}_2 + \boldsymbol{B}_1\boldsymbol{K}_2 & \boldsymbol{B}_1(\boldsymbol{\Gamma} - \boldsymbol{K}_1\boldsymbol{\Pi}_1 - \boldsymbol{K}_2\boldsymbol{\Pi}_2)\boldsymbol{\Sigma}^{-1} \\ \boldsymbol{0} & \boldsymbol{0} & (\boldsymbol{\Sigma S} - \boldsymbol{G\Pi}_1)\boldsymbol{\Sigma}^{-1}\end{bmatrix}\right) \subset \mathbb{C}^-.$$

Thus, the system has a locally attractive center manifold at $(\boldsymbol{\theta}_1, \boldsymbol{\theta}_2, \boldsymbol{z}, \boldsymbol{w}) = (\boldsymbol{0}, \boldsymbol{0}, \boldsymbol{0}, \boldsymbol{0})$, and the graph of a mapping $(\boldsymbol{\theta}_1, \boldsymbol{\theta}_2, \boldsymbol{z}) = \big(\boldsymbol{\pi}_1(\boldsymbol{w}), \boldsymbol{\pi}_2(\boldsymbol{w}), \boldsymbol{\sigma}(\boldsymbol{w})\big)$. This manifold is annihilated by the error map $\boldsymbol{e} = \boldsymbol{p}(\boldsymbol{\theta}_1) - \boldsymbol{q}(\boldsymbol{w})$. By continuity of $\boldsymbol{p}(\boldsymbol{\theta}_1)$, $\lim_{t\to\infty}\Big(\boldsymbol{p}\big(\boldsymbol{\theta}_1(t)\big) - \boldsymbol{q}\big(\boldsymbol{w}(\boldsymbol{t})\big)\Big) = \boldsymbol{0}$. ■

IV. Simulation and Discussion

A. Methods and procedures

The heart motion data used in this paper was from Case Western Reserve University. The data represents the motion of a point of interest on the heart of an adult pig with sampling rate of 257 Hz, Figure 1. Figure 2 shows frequency analysis of the above heart data where main fundamental frequencies of the heart motion were ω_r=2.146 rad/s and ω_c=12.591 rad/s respectively. Suppose the cycle was set as 1s. As the example, the period of 20s to 21s (Period I) was treated as the previous cycle while the reference signal to track in the current cycle was during the period of 21s to 22s (Period II), Figure 1. Then Period I of heart motion data was used to obtain the estimation of the fundamental frequencies where the coefficient vector was initialized as,

$$\hat{\boldsymbol{x}}(0) = [2.146\Delta T \quad 12.591\Delta T \quad \boldsymbol{0}_{1\times(2(N_r+N_c+2N_h)+1)}]^T$$

The frequencies in the coefficient vector were initialized according to the frequency analysis result of heart data, and other coefficients are initialized as zeroes. By LMA, the fundamental frequencies were identified as $\omega_r = 2.1698\,(\mathrm{rad/s})$ and $\omega_c = 12.5943(\mathrm{rad/s})$ during the period I. Simulations were conducted in Matlab@ and Simulink@. PHANToM@ robot was used to simulate the surgical robot where main elements of matrices in Eq. (6) are shown in Table 1 and Table 2 [14]. Other matrix elements are all zeroes. MPC in [6] was used for comparing with the proposed control algorithm.

B. Simulation results

Figure 3 shows the position tracking error of the end effector of the surgical robot in three dimensions for the proposed output regulator. The reference signal is the heart motion data during 20s and 25s in Figure 1. The root mean square of the tracking error is 0.2837 mm using the proposed method. It is also observed that there are several peaks on the tracking error curve. It is believed that those peaks were caused by the noise of the original ECG signal. Figure 4 shows the input torque using the proposed output regulation technique. According to Figure 4, the control efforts are relatively large at some peaks but still within the reasonable range. Figure 5 shows the position tracking error of the end effector of the surgical robot using the MPC method during the same period. The root mean square of the tracking error using the MPC method is 1.5290 mm. According to Figure 3 and Figure 5, the proposed output regulation method can achieve much better performance comparing to MPC method.

Note that the heart motion model consists of seven harmonics in in the simulation. More harmonics would result in more accurate performance. Modification of the heart model will be applied in the future work to further improve motion compensation performance.

Table 1. Matrices in dynamics model of PHANToM robot

$M_{11} = I_0 + I_1 \cos 2\theta_2 + I_2 \cos 2\theta_3 + 2I_3 \cos\theta_2 \sin\theta_3$
$M_{22} = I_4$
$M_{33} = I_5$
$M_{23} = M_{32} = -I_3 \sin(\theta_2 - \theta_3)$
$C_{11} = -J_0\dot{\theta}_2 - J_1\dot{\theta}_3$
$C_{12} = -C_{21} = -J_0\dot{\theta}_1$
$C_{13} = -C_{31} = -J_1\dot{\theta}_1$
$C_{23} = I_3 \cos(\theta_2 - \theta_3)\,\dot{\theta}_3$
$C_{32} = I_3 \cos(\theta_2 - \theta_3)\,\dot{\theta}_2$
$N_2 = T_0 \cos\theta_2$
$N_3 = T_1 \cos\theta_3$

Table 2. Parameters of PHANToM robot [16]

$I_0 = 28.328 \times 10^{-4}\mathrm{kg \cdot m^2}$	$I_1 = 11.319 \times 10^{-4}\mathrm{kg \cdot m^2}$
$I_2 = -3.9120 \times 10^{-4}\mathrm{kg \cdot m^2}$	$I_3 = 4.5615 \times 10^{-4}\mathrm{kg \cdot m^2}$
$I_4 = 24.264 \times 10^{-4}\mathrm{kg \cdot m^2}$	$I_5 = 9.3189 \times 10^{-4}\mathrm{kg \cdot m^2}$
$T_0 = 162.30 \times 10^{-4}\mathrm{N \cdot m}$	$T_1 = 734.47 \times 10^{-4}\mathrm{N \cdot m}$

V. CONCLUSION

This paper has proposed an output regulator as a control method for robotic-assisted surgery. The proposed control method does not require the exact reference signal, i.e. heart motion to achieve motion compensation during the surgery. Based on the real data from the pig heart, the proposed technique was simulation. Simulation results have illustrated effectiveness of the proposed output regulator comparing with the model predictive controller. Future work will focus on more accurate modelling for heart motion.

REFERENCES

[1] Y. Nakamura, K. Kishi and H. Kawakami, "Heartbeat synchronization for robotic cardiac surgery," In *Proceedings of IEEE International Conference on Robotics and Automation*, Seoul, Korea, 2001, pp. 2014--2019.

[2] A. Thakral, J. Wallace, D. Tomlin, N. Seth, and N. V. Thakor, "Surgical motion adaptive robotic technology (SMART): Taking the motion out of physiological motion," in *Proceedings of 4th International Conference of Medical Image Computing and Computer-Assisted Intervention*, Utrecht, The Netherlands, 2001, pp. 317--325.

[3] T. Ortmaier, M. Groger, D. H. Boehm, V. Falk, and G. Hirzinger, "Motion estimation in beating heart surgery," *IEEE Transactions on Biomedical Engineering,* vol. 52, no. 10, pp. 1729--1740, 2005.

[4] R. Ginhoux, J. Gangloff, M. de Mathelin, L. Soler, M. M. A. Sanchez, and J. Marescaux, "Active filtering of physiological motion in robotized surgery using predictive control," *IEEE Transactions on Robotics,* vol. 21, no. 1, pp. 67--79, 2005.

[5] J. Rotella, "Predictive tracking of quasi periodic signals for active relative motion cancellation in robotic assisted coronary artery bypass graft surgery," M.E. dissertation, Case Western Reserve University, Cleveland, OH, 2005.

[6] O. Bebek, "Robotic-assisted beating heart surgery," Ph.D. dissertation, Case Western Reserve University, Cleveland, OH, 2008.

[7] B. Cagneau, N. Zemiti, D. Bellot, and G. Morel, "Physiological motion compensation in robotized surgery using force feedback control," in *Proceedings of IEEE International Conference on Robotics and Automation,* Roma, Italy, 2007, pp. 1881-1886

[8] V. Duindam and S. Sastry, "Geometric motion estimation and control for robotic-assisted beating-heart surgery," in *Proceedings of IEEE Conference on Intelligent Robots and Systems*, San Diego, USA, 2007, pp. 871–876.

[9] S. G. Yuen, D. T. Kettler, P. M. Novotny, R. D. Plowes, and R. D. Howe, "Robotic motion compensation for beating heart intracardiac surgery," *The International journal of robotics research,* vol. 28, no.10, pp. 1355--1372, 2009.

[10] J. M. Florez, D. Bellot, J. Szewczyk, and G. Morel,

"Serial Comanipulation in Beating Heart Surgery Using a LWPR-Model Based Predictive Force Control Approach," in *Proceedings of 4th International Conference on Intelligent Robotics and Applications*, Aachen, Germany, 2011, pp. 389--400.
[11] W. Bachta, P. Renaud, E. Laroche, A. Forgione, and J. Gangloff, "Active Stabilization for Robotized Beating Heart Surgery," *IEEE Transactions on Robotics,* vol. 27, no. 4, pp. 757-768, 2011.
[12] R. Richa, A.P.L. Bo and P. Poignet, "Beating heart motion prediction for robust visual tracking," in *Proceedings of IEEE International Conference on Robotics and Automation*, Anchorage, USA, 2010, pp. 4579--4584.
[13] J. Jamsek, A. Stefanovska, and P. V. McClintock, "Nonlinear cardio-respiratory interactions revealed by time-phase bispectral analysis," *Physics in medicine and biology*, vol. 49, no. 18, pp. 4407--4426, 2004
[14] M. Cenk, D. Feygin and F. Tendick, "A Critical Study of the Mechanical and Electrical Properties of the PHANToM Haptic Interface and Improvements for High-Performance Control," *Presence Teleoperators Virtual Environments,* vol. 11, no. 6, pp. 555--568, 2002.
[15] A. Isidori and C. I. Byrnes, "Output regulation of nonlinear systems," *IEEE Transactions on Automatic Control,* vol. 35, no. 2, pp. 131--140, 1990.
[16] L. Marconi, A. Isidori and A. Serrani, "Autonomous vertical landing on an oscillating platform: an internal-model based approach," *Automatica,* vol. 38, no. 1, pp. 21--32, 2002.

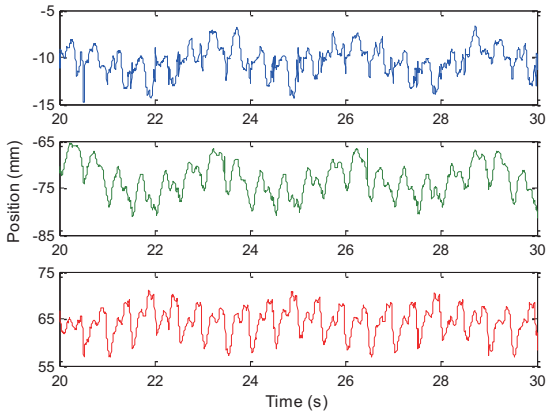

Figure 1. Portion of heart data from an adult pig

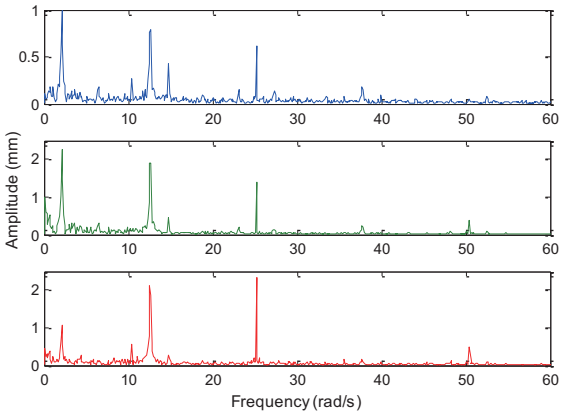

Figure 2. Frequency analysis of heart data

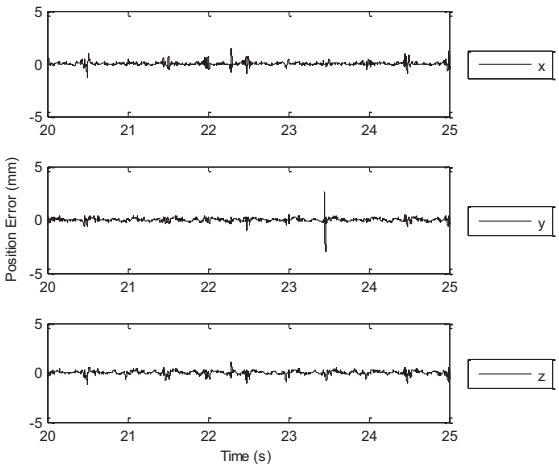

Figure 3. Position tracking errors using output regulator

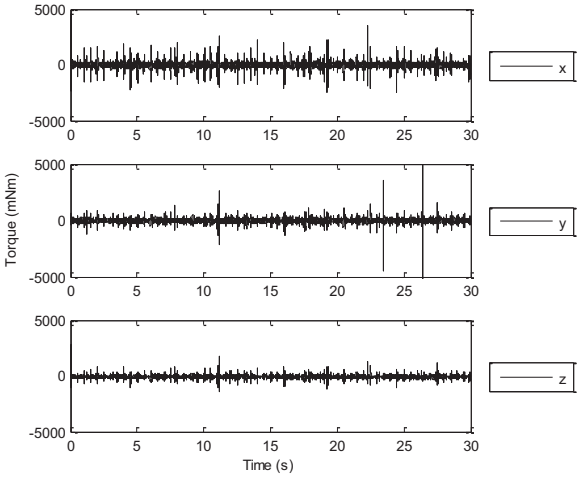

Figure 4. Torque input using output regulator

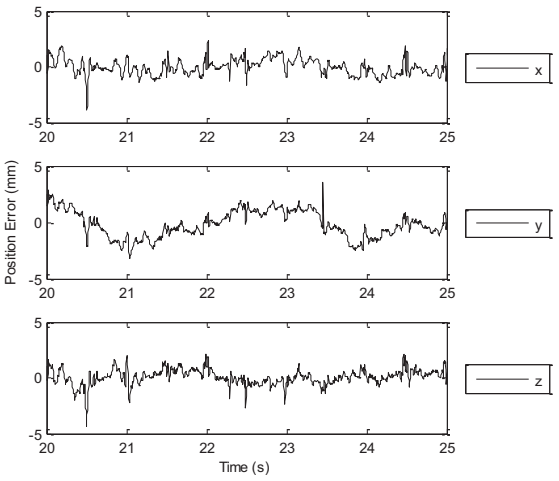

Figure 5. Position tracking errors using MPC